Plastic Hinge Rotation Capacity of Reinforced Concrete Beams

Ali Kheyroddin[1] **and Hosein Naderpour**[2]

[1] Associate Professor, Department of Civil Engineering, Semnan University, Semnan, Iran
[2] Ph.D. Candidate, Department of Civil Engineering, Semnan University, Semnan, Iran

Abstract: *A parametric study is performed to assess the influence of the tension reinforcement index, ($\omega = \rho f_y/f'_c$), and the bending moment distribution (loading type) on the ultimate deformation characteristics of reinforced concrete (RC) beams. The analytical results for 15 simply supported beams with different amounts of tension reinforcement ratio under three different loading conditions are presented and compared with the predictions of the various formulations and the experimental data, where available. The plastic hinge rotation capacity increases as the loading is changed from the concentrated load at the middle to the third-point loading, and it is a maximum for the case of the uniformly distributed load. The effect of the loading type on the plastic rotation capacity of the heavily reinforced beams is not as significant as that for the lightly reinforced beams. Based on the analytical results obtained using the nonlinear finite element method, new simple equations as a function of the tension reinforcement index, ω, and the loading type are proposed. The analytical results indicate that the proposed equations can be used for analysis of ultimate capacity and the associated deformations of RC beams with sufficient accuracy.*

Keywords: *Nonlinear Analysis, Finite Element, Plastic Hinge, Reinforced Concrete, Rotation Capacity*

1. Introduction

It is well established that the inelastic behavior of Reinforced Concrete (RC) sections leads to a redistribution of moments and forces, resulting in an increased load carrying capacity of the members and the indeterminate structure. As the applied load is increased, hinges start forming in succession at locations where the hinge moment capacity is reached; with further increase in the applied load, these hinges continue to rotate until the last hinge forms converting the structure into a mechanism resulting in failure.

Kheyroddin has reviewed the various limit design methods which have been proposed based on the concepts of limit equilibrium, serviceability, and rotational compatibility in terms of the available rotation at the plastic hinge being larger than the rotation required to form a collapse mechanism [1].

The plastic hinge rotation, θ_p, of RC beams depends on a number of parameters including the definition of yielding and ultimate curvatures, section geometry, material properties, compression and tension reinforcement ratios, transverse reinforcement, cracking and tension-stiffening, the stress-strain curve for the concrete in tension and compression, the stress-strain curve for the reinforcing steel, bond-slip characteristics between the concrete and the reinforcing steel, support conditions and the magnitude and type of loading, axial force, width of the loading plate, influence of shear, and the presence of column. Several researchers have investigated this problem; however, individual researchers differ even on the basic definition of what is to be taken as the plastic rotation capacity. Some of these

contradictions among the various researchers are partly due to the definition of the ultimate limit state, and the different test conditions such as the specimen dimensions, loading plate geometry, and the method of application and type of loads on the beam. Some equations have been proposed to calculate the plastic hinge length and the inelastic rotation capacity; however, there is no general agreement on the techniques to evaluate the inelastic behavioral characteristics of indeterminate concrete structures.

The conditions at the ultimate load stage of a typical cantilever beam subjected to uniform load are shown in Fig. 1. For values of loads smaller than the yielding moment, M_y, the curvature increases gradually from the free end of a cantilever (point A) to the column face (point B). There is a large increase in the curvature at first yield of the tension steel. At the ultimate load stage, the value of the curvature at the support increases suddenly so that it causes large inelastic deformations. Since the concrete between the cracks can carry some tension (tension-stiffening), the curvature fluctuates along the beam length. Each of the peaks of curvature corresponds to a crack location. The actual distribution of curvature at the ultimate load stage can be idealized into elastic and inelastic (plastic) regions [Fig. 1(c)], thus the total rotation, θ_t, over the beam length can be divided into elastic, θ_e, and plastic, θ_p, rotations. The elastic rotation, θ_e, (until yielding of steel) can be obtained using the curvature at yielding. With reference to Fig. 1, the plastic hinge rotation, θ_p, on each side of the critical section, can be determined as:

$$\theta_p = \int_0^{l_y} \left[\phi(x) - \phi_y\right] dx \qquad (1)$$

In which l_y is the beam length over which the bending moment is larger than the yielding

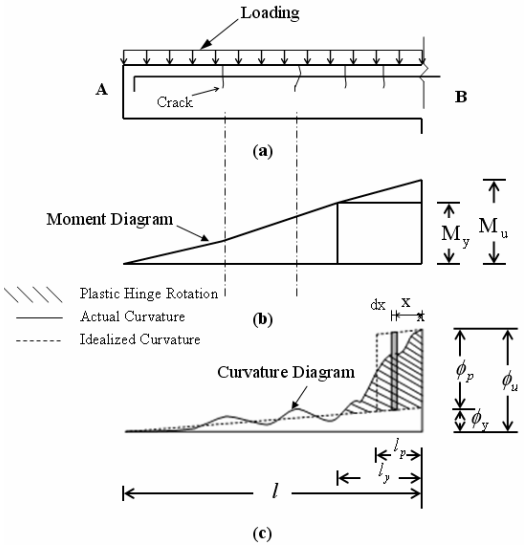

Fig.1 Schematic Curvature Distribution along Beam at Ultimate Stage:
(a) Beam, (b) Bending Moment Diagram,
(c) CurvatureDiagram

moment, M_y, or the distance between the critical section and the location where tension steel first yields (Fig. 1) and $\phi(x)$ is the curvature at a distance x from the critical section at the ultimate load stage.

The shaded area in Fig. 1(c) is the plastic (inelastic) rotation, θ_p that occurs in addition to the elastic rotation at the plastic hinge at the ultimate load stage. The plastic hinge rotation can be determined either by the calculation of shaded area or by an equivalent rectangle of height (ϕ_u–ϕ_y) and width l_p. Using Eq. 1, the equivalent plastic hinge length, l_p, can be defined as:

$$l_p = \frac{1}{\phi_u - \phi_y} \int_0^{l_y} \left[\phi(x) - \phi_y\right] dx \qquad (2)$$

Therefore, the value of plastic hinge rotation, θ_p, at ultimate stage can be calculated easily by the following well-known equation:

$$\theta_p = \left(\phi_u - \phi_y\right) l_p = \phi_p \, l_p \qquad (3)$$

Where ϕ_u and ϕ_y are the curvatures at the

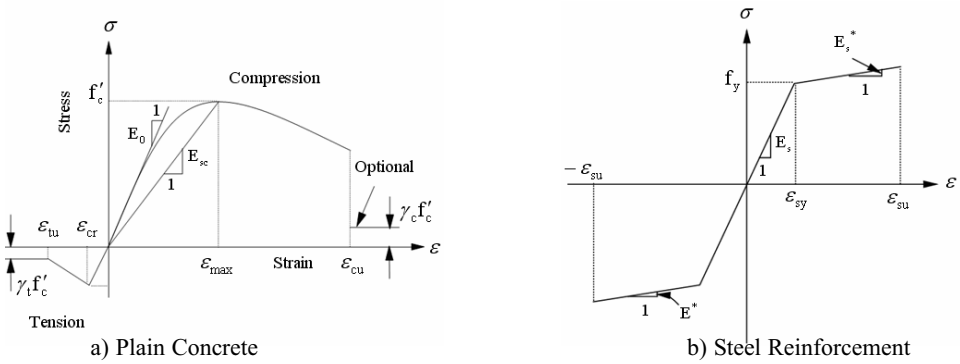

a) Plain Concrete b) Steel Reinforcement

Fig.2 Uniaxial Stress-Strain Curves

ultimate load and yielding, respectively and l_p is the equivalent length of the plastic hinge over which the plastic curvature, ($\phi_p=\phi_u-\phi_y$), is assumed to be constant. Equation 3 results in the same area as the actual plastic curvature distribution (Shaded area in Fig. 1). A survey of the literature shows that most researchers first calculate the equivalent plastic hinge length, l_p, and then the plastic rotation, θ_p, is determined using equation 3.

In this paper, a nonlinear layered finite element program is used for determination of the yielding length, plastic hinge length and the plastic hinge rotation. In fact, at first the plastic rotation is determined and then the equivalent plastic hinge length is derived only for comparison. The advantage of the present study is that the yielding length and the "exact" value of plastic rotation (shaded area in Fig. 1b) can be determined with more accuracy without using the concept of the equivalent plastic hinge length. Further, a parametric study is performed to examine the influence of tension reinforcement index and the loading type on the ultimate deformation characteristics of RC beams and new equations are developed to consider the influence of the various parameters on the calculation of the plastic hinge rotation. Attention is focused on the plastic rotation capacity at the ultimate limit state only.

2.Nonlinear Finite Element Program

A nonlinear finite element analysis program, NONLACS2 (NONLinear Analysis of Concrete and Steel Structures), developed by Kheyroddin [1], is used to analyze the selected RC beams. The program can be used to predict the nonlinear behavior of any plain, reinforced or prestressed concrete, steel, or composite concrete-steel structure that is composed of thin plate members with plane stress conditions. This includes beams, slabs (plates), shells, folded plates, box girders, shear walls, or any combination of these structural elements. Time-dependent effects such as creep and shrinkage can also be considered.

2.1. Concrete Properties

As shown in Fig. 2(a), the uniaxial stress-strain curve of concrete adopted in this study is made of two parts. The ascending branch up to the peak compressive strength is represented by the equation proposed by Saenz [2]:

$$\sigma = \frac{E_0 \varepsilon}{1+\left(\frac{E_0}{E_{SC}}-2\right)\left(\frac{\varepsilon}{\varepsilon_{\max}}\right)+\left(\frac{\varepsilon}{\varepsilon_{\max}}\right)^2} \quad (4)$$

Where E_0 is the initial modulus of elasticity of the concrete, E_{sc} is the secant modulus of

the concrete at the peak stress, σ is the stress, å is the strain, and ε_{max} is the strain at peak stress. The descending or the strain-softening branch is idealized by the Smith and Young model [3]:

$$\sigma = \sigma_c \left(\frac{\varepsilon}{\varepsilon_{max}} \right) exp(1 - \frac{\varepsilon}{\varepsilon_{max}}) \quad (5)$$

Where σ_c is the compressive strength of the concrete. For uniaxially loaded concrete, σ_c is equal to f'_c. For high-strength concrete, the compressive stress-strain response is modeled using a modified form of the Popovics' Equation (see [1]).

For analysis of most plane stress problems, concrete is assumed to behave as a stress-induced orthotropic material. In this study the orthotropic constitutive relationship developed by Darwin and Pecknold [4] is used for modeling the concrete using the smeared cracking idealization. The constitutive matrix, D, is given by:

$$D = \frac{1}{(1-\nu^2)} \begin{bmatrix} E_1 & \nu\sqrt{E_1 E_2} & 0 \\ \nu\sqrt{E_1 E_2} & E_2 & 0 \\ 0 & 0 & \frac{1}{4}(E_1 + E_2 - 2\nu\sqrt{E_1 E_2}) \end{bmatrix} \quad (6)$$

In which, E_1 and E_2 are the tangent module in the directions of the material orthotropy, and ν is the Poisson's ratio. The orthotropic material directions coincide with the principal stress directions for the uncracked concrete and these directions are parallel and normal to the cracks for the cracked concrete. The concept of the "equivalent uniaxial strain" developed by Darwin and Pecknold [4] is utilized to relate the increments of stress and strain in the principal directions. Therefore, stress-strain curves similar to the uniaxial stress-strain curves can be used to formulate the required stress-strain curves in each principal direction.

The strength of concrete, σ_c, and the values of E_1, E_2 and ν are functions of the level of stress, and the stress combinations. The concrete strength when subjected to biaxial stresses is determined using the failure envelope developed by Kupfer et al. [5]. The values of E1 and E2 for a given stress ratio ($\alpha = \sigma_1/\sigma_2$) are found as the slopes of the σ_1-ε_1 and σ_2-ε_2 curves, respectively. For the descending branches of both compression and tension stress-strain curves, E_i is set equal to a very small number, 0.0001, to avoid computational problems associated with a negative and zero values for E_i. The concrete is considered to be crushed, when the equivalent compressive strain in the principal directions exceeds the ultimate compressive strain of the concrete, ε_{cu}. For determination of the concrete ultimate compressive strain, ε_{cu}, two models for unconfined high and normal-strength concrete [6] and confined concretes [7] are implemented in the program.

For elimination of the numerical difficulties after crushing ($\varepsilon > \varepsilon_{cu}$) and cracking of the concrete ($\varepsilon > \varepsilon_{tu}$), a small amount of compressive and tensile stress as a fraction of concrete strength, $\gamma_c f'_c$ and $\gamma_t f'_t$, is assigned (optional) at a high level of stress [Fig. 2(a)], where parameters γ_c and γ_t define the remaining compressive and tensile strength factors, respectively.

Cracking of the concrete is idealized using the smeared cracking model, and is assumed to occur when the principal tensile stress at a point exceeds the tensile strength of the concrete.

2.2. Reinforcing Bar Properties

The reinforcing bars are modeled as an elastic strain-hardening material as shown in Fig. 2(b). The reinforcing bars can be modeled either as smeared layers or as individual bars. In both cases, perfect bond is

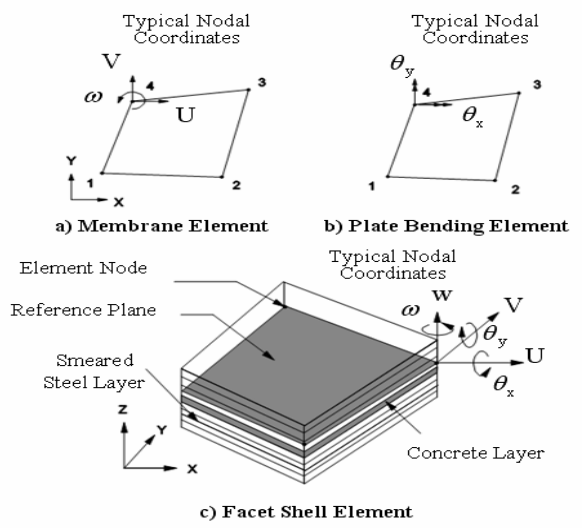

Fig.3 Some Typical Finite Elements in NONLACS2 Program

assumed between the steel and the concrete.

2.3. Finite Element Formulation

The element library includes plane membrane, plate bending, one dimensional bar, spring boundary elements as well as a facet shell element which is a combination of the plane membrane and the plate bending elements. Figure 3 shows some of these elements and the associated degrees of freedom. The program employs a layered finite element approach. The structure is idealized as an assemblage of thin constant thickness plate elements with each element subdivided into a number of imaginary layers as shown in Fig. 3(c). A layer can be either of concrete, smeared reinforcing steel or a continuous steel plate. Each layer is assumed to be in a state of plane stress, and can assume any state - uncracked, partially cracked, fully cracked, non-yielded, yielded and crushed - depending on the stress or strain conditions. Analysis is performed using an incremental-iterative tangent stiffness approach, and the element stiffness is obtained by adding the stiffness contributions of all layers at each Gauss quadrature point. The history, capability, element library, constitutive models and the limitations of the NONLACS2 program are presented by Kheyroddin [1].

3. Analysis of Reinforced Concrete Beam,C5

One simply supported beam, C5, subjected to a midspan-concentrated loading tested by Mattock [8] is analyzed using the NONLACS2 program and a finite element mesh with 88 elements (Fig. 4). This beam is also used for further parametric studies. The experimental material properties for the concrete and the reinforcing steel are presented in Table 1. Since the reinforcement and the loading are symmetrical with respect to the mid span, only one half of the beams is modeled. The vertical loads are applied in 30 load steps with smaller increments of loads being applied just before the beam reaches its ultimate load stage. This would improve the rate of convergence of the solution and the accuracy in predicting the ultimate load. The details of geometry, reinforcement, loading

Table 1. Dimensions and Properties of Beam C5

A_s (mm^2)	A'_s (mm^2)	f'_c (MPa)	E_0 (MPa)	ε_{cu}	f'_t (MPa)	f_y (MPa)	E_s (MPa)	E_s^* (MPa)	ε_{su}
1135.5	142.0	23.4	23145	0.0078	3.0	328.2	195130	5515	0.05

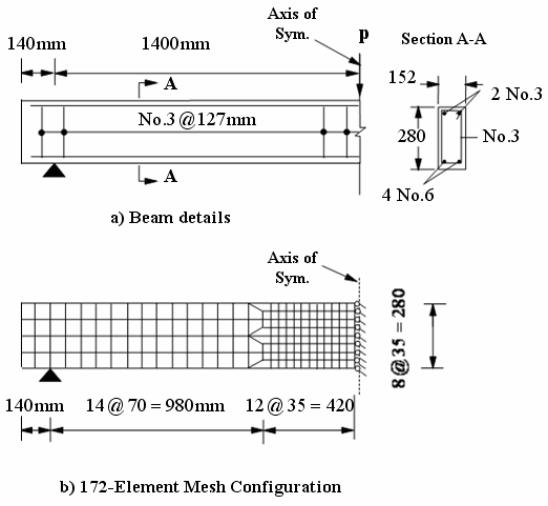

Fig.4 Geometry, Reinforcement Details and Mesh Configuration for Beam C5

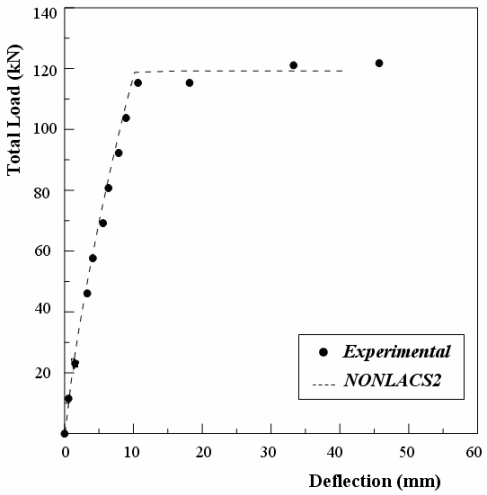

Fig.5 Comparison of Experimental and Analytical Results for Beam C5; Load-Deflection Curve

pattern and finite element modeling of this beam are shown in Fig. 4. Since this phenomenon represents a plane stress condition, only one layer of concrete is sufficient. The longitudinal reinforcements are lumped in a single bar at the reference surface as a bar element. The stirrups are modeled as smeared steel layers on the two sides of the beam.

In order to determine accurate values of the yielding length and plastic rotations near the critical section (midspan), a fine mesh configuration with 172 elements is utilized [Fig. 4(b)]. In other words, nonlinear finite element analysis of selected beams have been carried out using the NONLACS2 program using small elements (35×35 mm) in the neighborhood of the "critical" section, and progressively increasing to, 70×70 mm, elements in the neighborhood of the zero moment location at the support. To evaluate the accuracy of the 172-element model, beam C5 is analyzed using the NONLACS2 program. The load-deflection and moment-curvature curves obtained from the program are compared with the experimental findings in Fig. 5. The computed results from the beam idealization using 172 elements shows excellent agreement with the experimental results. In this model, the load corresponding to the initiation of crack in the structure is 14.23 kN, when the first crack occurs in the beam. The experimental values of loads for yielding of steel reinforcement and crushing of the concrete at the ultimate load are P_y=115.29 kN and P_u=121.79 kN, while the analytical yielding and ultimate loads are 118.76 kN and 119.2 kN, with discrepancies of +3 and -2 percent from experimental results, respectively, showing excellent agreement with the experimental results (Fig. 5.). The analytical yielding and ultimate deflections are 10.95 mm and 40.64 mm with

Table 2 Details of Mattock Beams Used in Parametric Study

Group No.	Beam	f'_c (MPa)	f_y (MPa)	ρ'	Parameters Studied	Type of Loading
1	M1jF	23.4	328.2	0.0037	ρ	Concentrated Loads
2	M2jF	23.4	328.2	0.0037	Loading Type	Uniform Loads
3	M3jF	23.4	328.2	0.0037	Loading Type	Third-Point Loadings

Table 3 Analytical Results Obtained Using the NONLACS2 Program (Group No. 1)

Beam	$\rho=A_s/bd$	$\omega=\rho f_y/f'_c$	Δ_y (mm)	Δ_u (mm)	$\mu_\Delta=\Delta_u/\Delta_y$	ϕ_y (10^{-5} rad/mm)	ϕ_u (10^{-5} rad/mm)	$\mu_\phi=\phi_u/\phi_y$	c (mm)	θ_p (rad)	l_y (mm)	l_p (mm)
M15F	0.0294	0.412	10.95	40.64	3.71	1.70	8.27	4.88	102.87	0.013	314.5	197.6
M14F	0.022	0.309	8.84	47.0	5.32	1.54	9.84	6.41	85.1	0.0148	332.7	178.1
M13F	0.0147	0.206	7.49	62.23	8.30	1.30	12.9	9.92	65.53	0.020	349.3	172.7
M12F	0.011	0.154	6.43	69.3	10.8	1.18	16.7	13.83	50.30	0.026	393.7	167.1
M11F	0.0074	0.103	5.59	84.3	15.1	1.02	22.4	21.9	37.08	0.034	402.6	158.8

a deviation of -4 and -13 percent from the experimental values of Δ_y=11.38 mm and Δ_u=46.74 mm, respectively.

4. Parametric Study

For the parametric study, the C5 Mattock beam, 152×280 mm (6 × 11 in), with a tension reinforcement index of 0.412 subjected to a mid-span concentrated load, is used in the study (Fig. 4). In addition, the same beam is analyzed with four other assumed tension reinforcement indices (0.309, 0.206, 0.154, and 0.103). Table 2 lists the parameters which are varied, together with their designations, cross sectional details, types of loading, concrete and steel strengths, for the 15 beams (3 Groups) investigated in this study. Each beam is designated as MijF, where "i" is the group number, "j" indicates the rank of the tension reinforcement ratio in increasing order, and "F" represents the use of the fine mesh with 172 elements.

5. Influence of Tension Reinforcement Index, ω

The loaddeflection curves obtained from the NONLACS2 program for the beams in Group No. 1, are shown in Fig. 6, which presents the results of five under-reinforced beams with different values of the tension reinforcement index ($\omega = \rho f_y/f'_c$). The analytical results including the yielding and ultimate deflections and curvatures, and ductility ratios for these beams are also presented in Table 3. The failure mode is flexural for all of the beams, i.e., steel yields first at the bottom at midspan and then the concrete crushes at the top of the beam at midspan. The cracking, yielding and the ultimate loads increase with the value of ω. The yielding deflection increases with an increase in the tension reinforcement index. An increase in ω by about 50 percent increases the yielding deflection by about 18 percent. The ultimate deflection and the deflection ductility ratio, $\mu_\Delta=\Delta_y/\Delta_u$ decrease with an increase in the tension

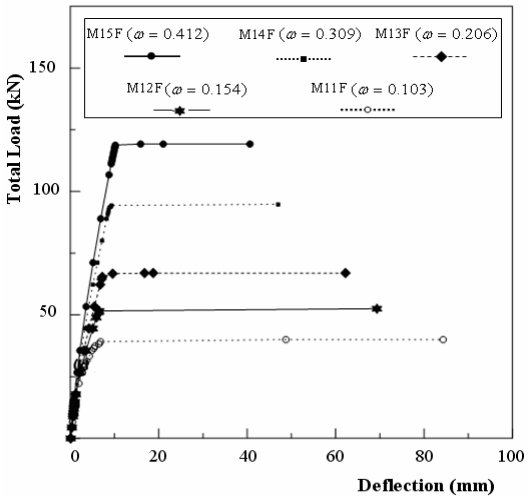

Fig.6 Load-Deflection Curves at Mid-Span for Beams with Different Reinforcement Index (Group No. 1)

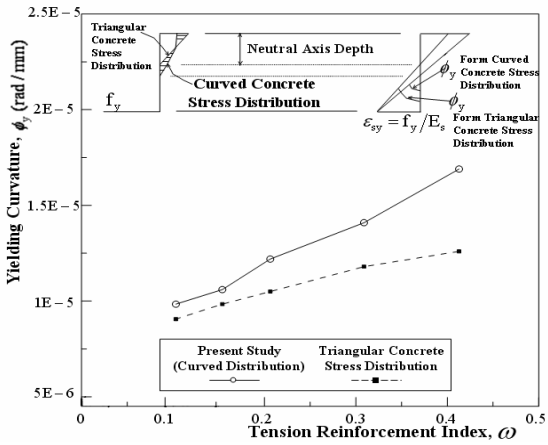

Fig.7 Variation of Yielding Curvature with Tension Reinforcement Index, ω

reinforcement index. The ultimate deflection for the beam M11F with ω=0.103 is 84.3 mm which is 79 percent higher than that for the beam M14F with ω = 0.309. The deflection ductility ratio varies between 3.71 to 15.1, as ω changes from 0.412 to 0.103.

5.1. Yielding Curvature

In reinforced concrete sections, the yielding curvature ϕ_y is well defined as a curvature when the tension reinforcement first reaches the yield strength, f_y. Most researchers (e.g. [9]) used a linear distribution of concrete stress and strain at the yielding stages (see Fig. 7). In a more accurate model, a nonlinear (curved) stress distribution should be used at the yielding stage, especially when the concrete compressive stress is high. As can be seen from Fig. 7, the value of neutral axis depth, c, calculated assuming a linear distribution of concrete stress is smaller than the "actual" value of the c if the concrete stress distribution is nonlinear, which would lead to an underestimation of the curvature at first yield, ϕ_y, and an overestimation of the curvature ductility ratio, $\mu_\phi=\phi_u/\phi_y$. Since the NONLACS2 program considers the nonlinear concrete compressive stress distribution, the yielding curvatures obtained from the program are about 9 to 35 percent greater than that the model assuming the linear stress distribution. For beam C5 (M15F) with ω=0.412, the analytical yielding curvature is 1.7×10^{-5} rad/mm which is very close to experimental value of 1.57×10^{-5}rad/mm with an 8 percent discrepancy, while the model with a linear stress distribution underestimates the yielding curvature by about 20 percent (ϕ_y=1.26×10^{-5} rad/mm). As the tension reinforcement index is increased, the yielding curvature increases and the difference between two models (linear and nonlinear stress distributions) increases.

5.2. Ultimate Curvature and Ductility Ratio

In the ACI 318-02 Building Code[10], the ultimate limit state is based implicitly on the assumption of a limit strain for concrete (ε_{cu}=0.003), while in CEB Model Code [11] it is based explicitly on both the steel and the concrete ultimate strains i.e. ε_{su}=0.01, and ε_{cu}=0.0035. Although the ultimate concrete strain values are satisfactory for the evaluation of the ultimate strength, they are very conservative for deformation analysis and moment redistribution. The ultimate steel strain limitation of ε_{su}=0.01 in the CEB

Table 4 Comparison of Existing ε_{cu} and θ_p Formulations (θ_p is the Plastic Rotation on One Side of Section)

Researcher(s)	Loading type	Expression for θ_p
Present study	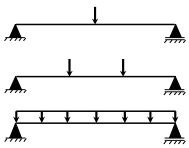	$\theta_p = \int_0^{l_p} [\phi(x) - \phi_y] dx$
Baker and Amarakone [16]	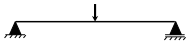	$\theta_p = 0.8(\varepsilon_{cu} - \varepsilon_{cy}) k_1 k_3 (\frac{z}{d})$; $(k_1 k_3 = 0.5)$ $\varepsilon_{cu} = 0.0015 [1 + 150 \rho_s + (0.7 - 10 \rho_s) \frac{d}{c}]$
Mattock [8]	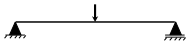	$\theta_p = (\phi_u - \phi_y \frac{M_u}{M_y})(1 + (1.14\sqrt{\frac{z}{d}} - 1)(1 - (\frac{\omega - \omega'}{\omega_b})\sqrt{\frac{d}{16.2}})) \frac{d}{2}$ $\varepsilon_{cu} = 0.003 + \frac{0.5}{z}$
Corley [17]	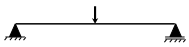	$\theta_p = (\phi_u - \phi_y \frac{M_u}{M_y})(1 + \frac{0.4}{\sqrt{d}} \frac{z}{d})(\frac{d}{2})$ $\varepsilon_{cu} = 0.003 + 0.02 \frac{b}{z} + (\frac{\rho_s f_y}{20})^2$
Riva and Cohn [18]	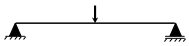	For $\frac{\phi_{pu}}{\phi_{py}} \le 7.0$: $\theta_p = (0.39 - \frac{7.0}{800\omega})(\frac{\phi_{pu}}{\phi_{py}})^{-0.9} \phi_{pu} z$ For $\frac{\phi_{pu}}{\phi_{py}} > 7.0$: $\theta_p = (\frac{5.4}{100}) \phi_{pu} z$
	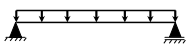	For $\frac{\phi_{pu}}{\phi_{py}} \le 7.0$: $\theta_p = (0.58 - \frac{3.0}{800\omega})(\frac{\phi_{pu}}{\phi_{py}})^{-0.9} \phi_{pu} z$ For $\frac{\phi_{pu}}{\phi_{py}} > 7.0$: $\theta_p = (\frac{5.0}{100} + \frac{6.5}{1000} \frac{\phi_{pu}}{\phi_{py}}) \phi_{pu} z$

Model Code [11] is excessively conservative, while the absence of a steel strain limitation in the ACI 318-02 [10] and the CSA Standard CSA A23.3-M94 [12] is unconservative. The most common definition adopted in the literature is that the ultimate limit state corresponds to the maximum moment capacity of the section (i.e. $\partial M / \partial \phi = 0$).

Based on the experimental data reported by Mattock [8], the concrete ultimate compressive strain, åcu, is selected equal to 0.0078. The most widely used ε_{cu} formulations available in the literature are presented in Table 4. The values of ε_{cu}=0.0057, ε_{cu}=0.012, and ε_{cu}=0.00645 have been adopted from the works of Baker and Amarakone, Mattock, and Corley (see Table 4).

Figure 8 shows the variation of analytical ultimate compressive concrete strain, ε_{cu}, at the top and the ultimate tensile steel strain, ε_{su}, at the bottom at midspan with respect to ω for beams in Group No. 1. The ultimate compressive strain of concrete is larger than 0.0082 and can be as high as 0.0085. The values of ε_{cu} and ε_{su} decrease with an increase in the value of ω. Riva and Cohn [13] arrived at a similar conclusion from their analyses. As can be seen from Baker and Amarakone's equation (Table 4), with an increase in the tension reinforcement index, the neutral axis depth, c, increases and consequently the value of åcu decreases. All other equations for ε_{cu} estimate constant values of ε_{cu} regardless of the amount of tension reinforcement index. The ultimate

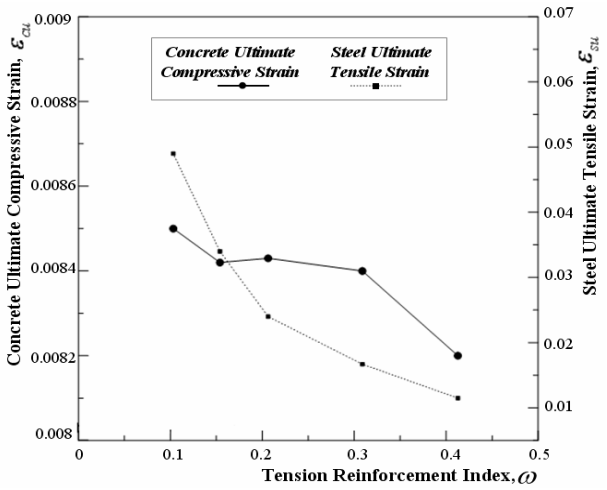

Fig.8 Effect of ω on Ultimate Concrete and Reinforcing Steel Strains (Group No. 1)

steel tensile strain at the bottom of the beams at midspan, as shown in Fig. 8, varies from 0.0115 to 0.049, as the tension reinforcement index changes from 0.412 to 0.103.

The neutral axis depth, c, is determined from the compatibility of the strains at the section. The ultimate curvature is then calculated as the ratio of ultimate concrete compressive strain at the top of beam to the neutral axis depth when the failure of structure occurs, i.e. $\phi_u=\varepsilon_{cu}/c$. The influence of the tension reinforcement index on the ultimate curvature and curvature ductility ratio, $\mu_\phi=\phi_u/\phi_y$ for Group No. 1 are shown in Figures 9 and 10, respectively. For comparison, the ultimate curvatures obtained using NONLACS2 program, Mattock's equation (Table 4), Corley's equation (Table 4) and the ACI method are presented. The neutral axis depth for each method is calculated based on the assumptions relevant to the method. For a given z/d ratio, the ultimate curvature decreases with an increase in the tension reinforcement index. The curvature is inversely proportional to the depth of the neutral axis, c, which varies directly as the tension reinforcement index at the ultimate limit state. The analytical results are about 2.35, 1.31, and 0.84 times the values obtained from the ACI, Corley's, and Mattock's methods, respectively. The ACI 318-02 Building Code [10] predicts the ultimate curvature very conservatively as compared with the other methods. Although the ultimate concrete compressive strain value, ε_{cu}=0.003, is satisfactory for the ultimate strength design, it is very conservative for deformation analysis. Mattock's method overestimates the ultimate curvature compared with the analytical results, because the concrete ultimate compressive strain determined by Mattock's equation (Table 4) is about 54 percent greater than the analytical concrete compressive strain value. For beam C5 (M15F), the value of ϕ_u using NONLACS2 program is equal to 8.3×10^{-5} rad/mm, while the ACI, Corley's, and Mattock's methods result in values of 2.4×10^{-5} rad/mm, 5.5×10^{-5} rad/mm, and 9.3×10^{-5} rad/mm, respectively. The experimental value of the ultimate curvature for this beam as reported by Mattock [8] is equal to 11.8×10^{-5} rad/mm, respectively.

As can be seen from Fig. 10, the curvature ductility ratio varies from 4.88 to 21.9, when the value of ω changes from 0.412 to 0.1. The figure shows that the curvature ductility ratios for the various methods are distributed

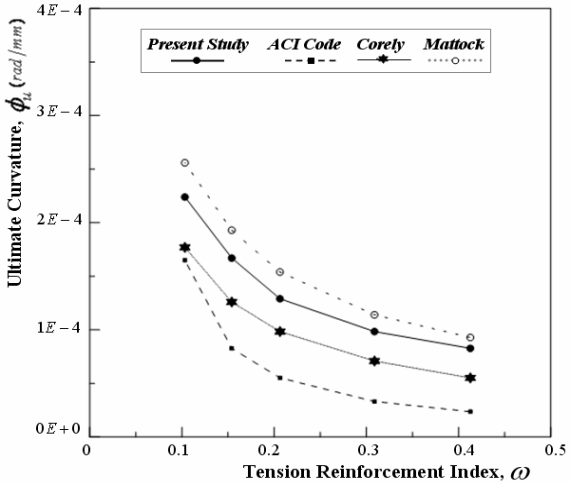

Fig.9 Variation of Ultimate Curvature with Respect to Tension Reinforcement Index, ω (Group No. 1)

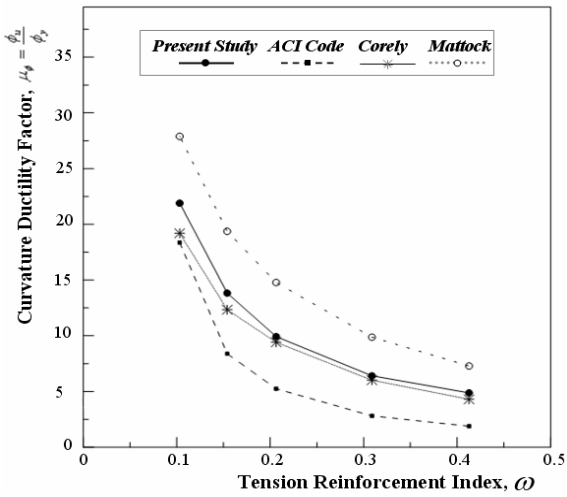

Fig.10 Effect of Tension Reinforcement Index on the Ductility Factor (Group No.1)

in the same manner as the ultimate curvatures calculated using the same methods. This was expected because the yield curvature is about the same for all of the methods. The ACI Code underestimates the curvature ductility ratio (up to 2.5 times) compared with the analytical results. For beam C5 (M15F), the analytical, the ACI, Corley's, and Mattock's methods have discrepancies of -36, -75, 44, and -5 percent from the experimental value of $\mu_\phi = 7.65$ (Fig.10).

5.3. Plastic Hinge Rotation and Length

Figure 11 illustrates the method to determine the analytical plastic rotation and the equivalent plastic hinge length for the beam M13F. First, the curvature along the beam is obtained from the concrete strain values in the compression zone and from the steel strain in tension zone at the ultimate limit state. Then, the plastic rotation, θ_p, is obtained by integration, along the yielding length, l_y (where the curvature in the section is higher than its yielding curvature, ϕ_y), of the difference between the ultimate curvature and the yielding curvature (Table 4). Here, θ_p refers to the plastic hinge rotation on one side of the critical section. Finally, the equivalent plastic hinge length, l_p, can be calculated as shown in Fig. 11(b).

The failure mechanism of beam M13F including the cracking of the concrete (solid lines) and its crushing (small circles) is shown in Fig. 11(a). The crushing of the concrete is concentrated at the top near the midspan or the critical section where the spread of inelasticity commences. The curvature increases linearly from the support to the yielding point and then the curvature suddenly increases and in the crushing region, it is very close to the ultimate curvature.

The spread of plasticity (yielding length), ultimate curvature and consequently the plastic rotation for the lightly reinforced beam (M12F) are greater than that for heavily reinforced beam (M15F). Comparison of the beams M12F and M15F indicates that an increase in ω by about 2.68 times decreases the yielding length and the plastic rotation by about 20 percent and 50 percent, respectively (Table 3).

A comparison of the analytical plastic rotation obtained from the NONLACS2 program with some models available in the

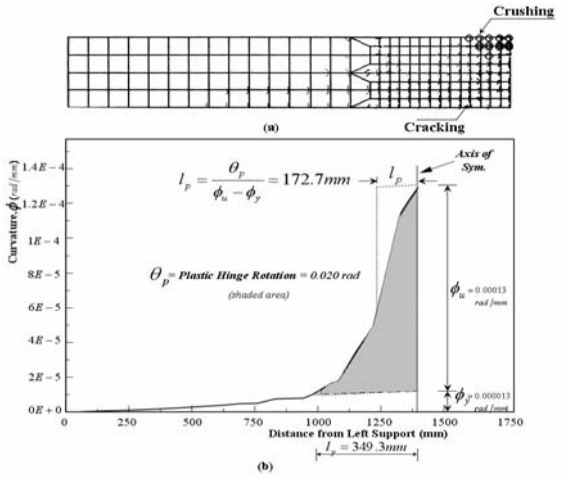

Fig.11 Calculation of Plastic Rotation for Beam M13F (ω =0.206) at Ultimate Stage: (a) Crack Pattern and Crushing of Concrete, (b) Plastic Hinge Rotation

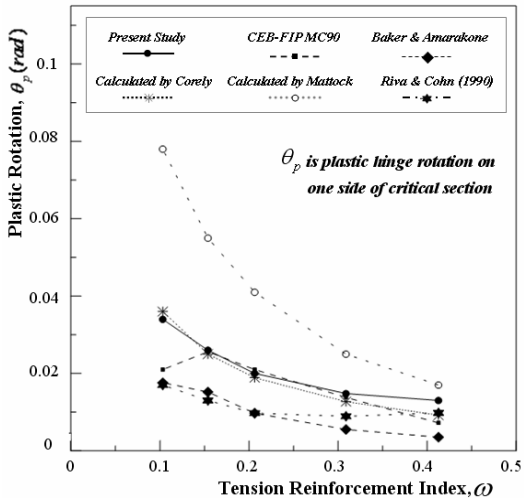

Fig.12 Comparison of Existing Plastic Hinge Rotation Formulations for Simply Supported Beams Subjected to Concentrated Load at Midspan (z/d=5.5)

literature is made here. The most widely used θ_p formulations in Europe and North America along with the formula used in the present study are presented in Table 4. The plastic rotations for the beams in Group No. 1 with z/d=5.5 using the NONLACS2, CEB-FIP MC90 [14], Baker and Amarakone's, Corley's, Mattock's and Riva and Cohn's methods are plotted in Fig. 12. Since the CEB, Corley, Mattock and Baker and Amarakone expressions in Table 4 are based on experiments mostly characterized by $z/d \approx 5.0$, and Riva and Cohn expression is valid for any z/d values, therefore a comparison among these models is reasonable. It is noted that the plastic hinge rotation obtained from Riva and Cohn's model (Table 4) is the total inelastic rotation from the onset of inelastic behavior, i.e. cracking of concrete. For all of the other methods including the present study, the plastic hinge rotation is defined as the rotation between the yielding and the ultimate states. The parameters ϕ_{pu} and ϕ_{py} in Riva and Cohn's formula are measured from the onset of cracking (ϕ_{cr}) and are determined using the NONLACS2 program. Compared with the CEB-FIP MC90 [14], the analytical results and Corley's theory are found to give safe values except in one case (ω =0.1) and yet they are not as conservative as Baker and Amarakone's and Riva and Cohn's formulations. For ω values greater than 0.15, the analytical results are close to the values obtained from CEB-FIP MC 90. The first branch of the CEB-FIP MC90 curve with a positive slope represents the failure of the tension reinforcement, and the second branch, with negative slope, indicates failure through the crushing of the concrete. The plastic rotation capacity predicted by the formula given by Riva and Cohn appear to represent a fairly safe estimate of the actual rotation capacities available up to the maximum load. Mattock's equation gives much higher values of the plastic rotation compared with any other models considered; this indicates that the expression given by Mattock for calculation of ε_{cu} tends to overestimate the deformability of RC sections. For beam C5 (M15F), the experimental plastic hinge rotation is 0.0249 rad, while the present study results in a value of 0.013 rad. The CEB, Baker and Amarakone's, Corley's, Mattock's and Riva and Cohn's methods predict plastic hinge

rotation values of 0.0072 rad, 0.0035 rad, 0.0092 rad, 0.017 rad, and 0.0098 rad, respectively.

The above comparison indicates that the experimental value is much higher than any other models considered. The experimental plastic rotation as reported by Mattock [8] was obtained from the measured inelastic deflection, δ_p, at midspan. The plastic rotation was assumed to be concentrated at the point of the maximum moment, and was equal to $\tan^{-1}(\delta_p / z)$. In fact, this assumption overestimated the plastic rotation and is independent of the shape of the bending moment diagram. Comparison of Mattock's experimental results with the experimental work of other researchers [15] corroborates the finding that Mattock's method results in much higher plastic rotations.

After calculation of the plastic hinge rotation, the analytical equivalent plastic length, l_p, on one side of critical section can be determined. As mentioned earlier, this value is obtained only for comparison with the other available methods. As can be seen from Table 3, the analytical value of l_p is not constant for the different values of the tension reinforcement indices. It increases linearly from 158.8 mm to 197.6 mm, as the value of ω changes from 0.103 to 0.412. The average value of the analytical plastic hinge length l_p is 174.9 mm, which is 69 percent of effective depth (0.69 d). In the new equation proposed by Baker and Amarakone (Table 4), l_p increases linearly with the *c/d* ratio. Riva and Cohn's formulation result in the lowest values of plastic hinge length and approximately the same pattern as the analytical curve. The Corley's, Mattock's, and Sawyer's theories give a constant plastic hinge length regardless of the reinforcement index, of 215.4 mm (0.85 d), 196.9 mm (0.78 d), and 168.2 mm (0.66 d), respectively. Based on the above discussion, it can be concluded that the rotation capacity of the plastic hinges in RC beams can be predicted using NONLACS2 program with sufficient accuracy.

6. Influence of Bending Moment Distribution (Loading Type)

In order to study the effect of the loading type, three loading conditions are considered: (1) concentrated load at midspan (linear moment distribution) to achieve a rapid moment variation as is observed at the supports in continuous beams, (2) third-point loading (linear moment distribution from the support to the location of the load and a constant moment between two loads), and (3) uniformly distributed loading (nonlinear moment distribution). The influence of the bending moment distribution on the plastic hinge rotation for Group Nos. 1, 2, and 3 is shown in Fig. 13. For these groups, all of the variables are the same, and the only difference is in the type of loading. The plastic hinge rotation increases as the loading type is changed from the midspan concentrated load, to the third-point loading, and it is a maximum for the case of the uniform load. The plastic hinge rotation for beams subjected to uniform loads are always greater than that for the same beams under third-point loadings or concentrated load.

As can be seen from Fig. 13, θ_p values for the beam subjected to third-point loading are larger than that for the beam loaded at midspan, when the value of ω is less than 0.38. Beyond $\omega = 0.38$, the value of θ_p for third-point loaded beam tends to be slightly less than the corresponding values for the beam loaded at midspan. In fact, the plastic rotation for the third-point loading depends on the length of constant moment region and

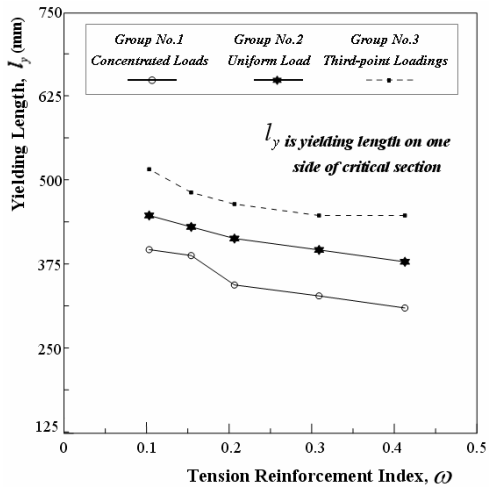

Fig.13 Influence of Different Loading Types on the Plastic Rotation

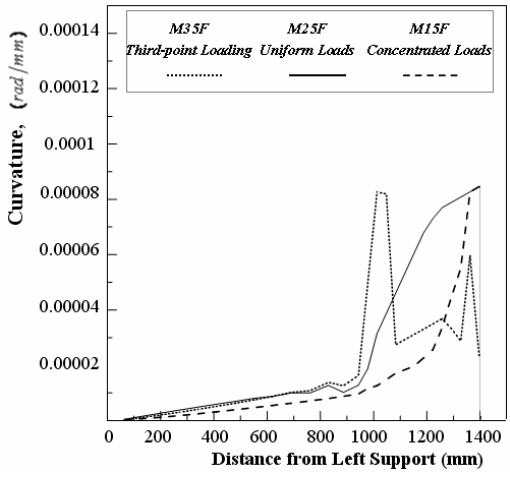

Fig.14 Variation of Yielding Length with Respect to Tension

the location of the plastic zone and the crushing of the concrete within a narrow area. This phenomenon will be explained latter. Bosco et al. [19] compared the plastic hinge rotations of simply supported beams under two different loading conditions: (1) three loads applied symmetrically with respect to the midspan, and (2) midspan concentrated load. They arrived at the same conclusion as in the present study. The plastic hinge rotations of lightly reinforced beams under three point loads were higher than that the beams loaded under central loads, while in the heavily reinforced beams, the plastic hinge of concentrated loaded beams were greater.

For two extreme values of ω, the effect of the loading type is discussed. For beam with $\omega = 0.103$, uniformly distributed loads on a simply supported beam lead to θ_p values varying from 1.90 to 1.35 times as high as those corresponding to the beams loaded with a midspan concentrated load or a third-point loading on the same beam, respectively. These ratios for the heavily reinforced beam with $\omega = 0.412$ are 1.59 and 0.88. Thus it can be concluded that the effect of the loading type on the plastic rotation capacity of heavily reinforced beams is not as significant as for the lightly reinforced beams. For the beam M81F (ω = 0.412), Riva and Cohn's formula (Table 4, for uniform loads) predicts the plastic hinge rotation equal to 0.064 rad, which is very close to the analytical value of 0.070 rad.

The variation of θ_p values for the differently loaded beams can be explained by the differences in the bending moment diagram and the yielding length, l_y, for each type of loading. Figure 14 shows that, with the same tension reinforcement index, the yielding length of the beam under a central load is less than that under uniform or third-point loads, leading to a smaller plastic rotation. Beams under uniform load show a considerable increase in the yielding length and the zone of plasticity. This is due to the smaller moment gradient (nonlinear moment distribution) in the neighborhood of the critical section.

On the other hand, the bending moment distribution will also influence the distribution of curvature along the length of the beam. Figure 15 shows the variation of curvature over half length of beams with

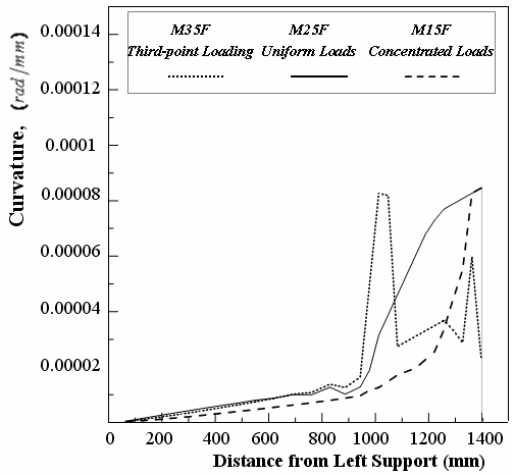

Fig.15 Effect of Loading Type on the Plastic Rotation of Beam with ω =0.412

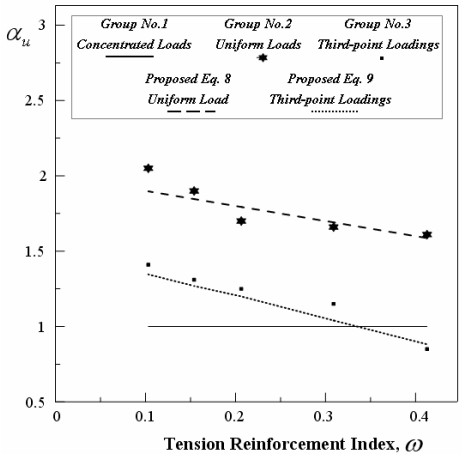

Fig.16 Analytical and Estimated Values of Plastic Rotations

ω =0.412 subjected to different loading types. Although the yielding length for the beam subjected to third-point loading is higher than that for the beams subjected to uniform and concentrated loads, localization of the plastic zone and the crushing of concrete, cause a smaller value of θ_p even less than that the beam subjected to concentrated load.

Although it has become common practice to use the terms "plastic hinge" and "critical section" or concentration of plastic rotations at the critical sections, the properties of the plastic hinge are not the properties of individual critical sections but they represent integrated curvature values over the length of the plastic hinge. As shown here, the loading type has a significant effect on the plastic hinge rotation and length, and the assumption of a constant plastic hinge length implies that the effects of the structural layout, magnitude and the type of load on the inelastic rotation have been neglected.

6.1. Proposed Equations

The relationship between the three different loading types at the ultimate load stage can be defined as:

$$\alpha_{u(Unif.)} = \frac{\theta_{p(Unif.)}}{\theta_{p(Conc.)}} = \frac{l_{p(Unif.)}}{l_{p(Conc.)}}$$
$$\alpha_{u(Third.)} = \frac{\theta_{p(Third.)}}{\theta_{p(Conc.)}} = \frac{l_{p(Third.)}}{l_{p(Conc.)}} \quad (7)$$

Where α_u is the loading type factor at the ultimate load stage. The variation of α_u with respect to the tension reinforcement index is shown in Fig. 16. Regression analysis of the results of the parametric study shows that the loading type factor can be expressed in term of the tension reinforcement index as:
For uniform loads, with $0.1 \leqq \omega \leqq 0.4$:

$$\alpha_{u(Unif.)} = (2.0 - \omega) \quad (8)$$

For third-point loadings, with $0.1 \leqq \omega \leqq 0.4$:

$$\alpha_{u(Third.)} = 1.5(1.0 - \omega) \quad (9)$$

The analytical values of the plastic hinge rotations obtained from the NONLACS2 program, $\theta_{p(anl)}$, and the values estimated using equations 6.2 and 6.3, $\theta_{p(est)}$, are compared in Table 5. The comparison is based on the relative error which is defined as:

$$ERR = \frac{\theta_{p(est.)} - \theta_{p(anl.)}}{\theta_{p(anl.)}} \quad (10)$$

Table 5 Analytical and Estimated Values of Plastic Rotation, θ_p (rad), for Different Loading Types.

$\omega = \rho f_y / f'_c$	Group No. 1 (Concentrated Loads)	Group No. 2 (Uniform Loads)			Group No. 3 (Third-Point Loadings)		
	NONLACS2	NONLACS2	Estimated (Eq. 8)	ERR %	NONLACS2	Estimated (Eq. 9)	ERR %
0.412	0.013	0.021	0.0206	-1.90	0.011	0.0114	3.63
0.309	0.0148	0.0245	0.025	2.04	0.017	0.0153	-9.76
0.206	0.020	0.034	0.0359	5.59	0.025	0.024	-4.0
0.154	0.026	0.0494	0.048	-2.83	0.034	0.033	-2.9
0.103	0.034	0.070	0.065	-7.14	0.048	0.046	-4.17

The maximum error between analytical and estimated values is 9.76 percent. The average value of the ratios of the proposed - to - analytical value of the plastic rotations for the beam subjected to uniform loads is found to be 0.991 with a standard deviation of 0.0486. The average value and the standard deviation for the proposed - to - analytical plastic rotations ratio for beam under third-point loadings are 0.965 and 0.0485, respectively. This indicates that the proposed equation predictions are in good agreement with the analytical results as shown in Fig.16. As a final remark, it is worth nothing that the reinforcement index and the type of loading are important factors to be considered in evaluating the rotation capacity of plastic hinges. The proposed equations can be used in any limit design method to evaluate the plastic hinge rotations and other deformation characteristics at the ultimate load when the statically indeterminate system transforms into a collapse mechanism.

7. Conclusions

Based on the analytical results, the following conclusions can be drawn:

1. The cracking, yielding and the ultimate loads increase with the tension reinforcement index, ω. The ultimate deflection and the deflection ductility ratio, $\mu_\Delta = \Delta_u / \Delta_y$, decrease with an increase in the value of ω. The deflection ductility ratio varies between 3.71 to 15.1, as ω changes from 0.412 to 0.103.

2. At the yielding stage, the value of the neutral axis depth, c, is smaller than the "actual" value of the depth of the compression zone, c, if the concrete stress distribution is assumed to be nonlinear, which will lead to an underestimation of the curvature at the first yield, ϕ_y, and an overestimation of the curvature ductility ratio, $\mu_\phi = \phi_u / \phi_y$.

3. At the ultimate load stage, the values of ε_{cu} and ε_{su} decrease with an increase in the value of ω. For a given z/d ratio, the ultimate curvature decreases with an increase in the tension reinforcement index. The analytical ultimate curvatures are about 2.35, 1.31, and 0.84 times the values obtained using the ACI, Corley's, and Mattock's methods, respectively.

4. The Corley's, Mattock's, and Sawyer's theories give a constant plastic hinge length regardless the reinforcement index, while the analytical value of l_p and the value of l_p obtained from Baker and Amarakone's, and Riva and Cohn's formulations is not constant for different values of tension reinforcement

indices. The average value of the analytical plastic hinge length on one side of the critical section is 69 percent of the effective depth.

5. The plastic hinge rotation increases as the loading is changed from the concentrated load to the third-point loading, and it is a maximum for the case of the uniformly distributed load. For the beam with ω=0.103, uniformly distributed loads on a simply supported beam lead to θ_p values varying from 1.90 to 1.35 times as high as those corresponding to the beams loaded with a midspan concentrated load or a third-point loadings on the same beam, respectively. It can be concluded that the effect of the loading type on the plastic rotation capacity of the heavily reinforced beams is not as significant as that for the lightly reinforced beams. It is concluded that the reinforcement index and the loading type have a significant effect on the plastic hinge rotation and length.

6. The analytical results indicate that the NONLACS2 program and the proposed equations (as a function of tension reinforcement index, ω, and the loading type) can be used for analysis of the ultimate capacity and the associated deformations of RC beams with sufficient accuracy.

8. References

[1] Kheyroddin, A., (1996). "Nonlinear Finite Element Analysis of Flexure-Dominant Reinforced Concrete Structures", Ph.D. Thesis, Department of Civil Engineering and Applied Mechanics, McGill University, Montreal, Canada, 290p.

[2] Saenz, L.P. (1965). "Equation for the Stress-Strain Curve of Concrete in Uniaxial and Biaxial Compression of Concrete", ACI Journal, V. 61, No. 9, pp. 1229-1235.

[3] Smith, G. M., and Young, L. E. (1955). "Ultimate Theory in Flexure by Exponential Function", Journal of American Concrete Inst., V. 52, No. 3, pp. 349-359.

[4] Darwin, D., and Pecknold, D.A. (1977). "Nonlinear Biaxial Stress-Strain Law for Concrete", ASCE Journal of the Engineering Mechanics Division, V. 103, No. EM4, pp. 229-241.

[5] Kupfer, H. B., Gerstle, K. H., and Rüsch, H. (1969). "Behavior of Concrete under Biaxial Stresses," Journal of ACI, V. 66, No. 8, pp. 656-666.

[6] Pastor, J.A. (1986). "High-Strength Concrete Beams", Ph.D. Thesis, Cornell University, New York, Ithaca.

[7] Scott, B.D., Park R., and Priestly, M.J.N. (1982). "Stress-Strain Behavior of Concrete Confined by Overlapping Hoops at Low and High Strain Rates", ACI Journal, V. 79, No. 1, Jan./Feb., pp. 13-27.

[8] Mattock, A.H. (1964). "Rotational Capacity of Hinging Regions in Reinforced Concrete Beams", Proceedings of the International Symposium on Flexural Mechanics of Reinforced Concrete, Miami, Florida, ACI SP-12, pp. 143-181.

[9] Park, R., and Paulay, T. (1975). "Reinforced Concrete Structures", John Wiley and Sons, New York.

[10] ACI Committee 318 (2002). "Building Code Requirements for Structural Concrete (ACI 318-02) and Commentary (ACI 318R-02)", American Concrete Institute, Farmington-Hills, Michigan, 2002, 443 p.

[11] CEB-FIP (1978), "Model Code for Concrete Structures", Paris.

[12] Canadian Standards Association (1994), Code for the Design of Concrete Structures for Buildings. CAN3-A23.3-M94, Rexdale, ON.

[13] Riva, P., and Cohn, M.Z. (1990), "Engineering Approaches to Nonlinear Analysis of Concrete Structures", ASCE J. Struct. Engng. Div., V. 116, No. 8, pp. 2162-2186.

[14] CEB-FIP Model Code 1990- Chapter 1-3, Final Draft. CEB Bull.d' Inf., 1991, No. 203.

[15] Siviero, E. (1974). "Rotation Capacity of Mono Dimensional Members in Structural Concrete", CEB Bull. d'Inf., No. 105, pp. 206-222.

[16] Baker, A.L.L., and Amarakone, A.M.N. (1964). "Inelastic Hyper Static Frames Analysis", Proceedings of the International Symposium on Flexural Mechanics of Reinforced Concrete, Miami, Florida, ASCE 1965-50, ACI SP-12, pp. 85-142.

[17] Corley, W.G. (1966). "Rotation Capacity of Reinforced Concrete Beams", Proceedings of the ASCE Structural Journal, V. 92, No. ST-4, pp. 121-146.

[18] Riva, P., and Cohn, M.Z. (1994). "Rotation Capacity of Structural Concrete Members", Magazine Concrete Research, V. 46, No. 168, pp. 223-234.

[19] Bosco, C., Carpinteri, A., and Debernardi, P.G. (1990). "Fracture of Reinforced Concrete: Scale Effects and Snap-Back Instability", Engng. Fracture Mechanics, V. 35, pp. 665-677.

[20] Shayanfar, M.A., Kheyroddin, A., and Mirza, M.S. (1997), "Element Size Effects in Nonlinear Analysis of Reinforced Concrete Members", Computers & Structures, Vol.62, No.2, 339-352.

[21] Bazant, Z. P., and Nova´k, D. (2000). "Energetic-Statistical Size Effect in Quasi-Brittle Failure at Crack Initiation", ACI Mater. J., 97(3), 381–392.

[22] Hillerborg, A. (1990). "Fracture Mechanics Concepts Applied to Rotational Capacity of Reinforced Concrete Beams", Eng.Fract.Mech, 53(1/2/3), 233–240.